

Chapter 5

Taming nonlinear dynamics with MLC

“Prediction is very difficult, especially about the future.”

- Niels Bohr

Frequency crosstalk is a ubiquitous phenomenon of turbulence and is of pivotal importance in control. In the *normal turbulence cascade*, the coherent structures feed increasingly smaller scales corresponding to increasingly larger frequencies with energy via the transfer term. In the *inverse cascade*, the merging of coherent structures yield increasingly larger scales or lower frequencies. All frequencies change the base flow, i.e. low frequencies, via the Reynolds stress. Thus, interacting frequencies range from the zero frequency corresponding to the mean flow to large frequencies corresponding to the Kolmogorov scale.

Control design may exploit this frequency crosstalk. Numerous experiments have demonstrated how high-frequency forcing can stabilize the fluid flow. Examples include jets [235], mixing layers [206], wakes [263], car models [21], and the flow over a backward-facing step [271]. Low frequency forcing can have a similar effect [209, 5]. In both cases, the coherent structures at a characteristic frequency are mitigated by a different imposed frequency. In other words, frequency crosstalk is a control enabler!

In this chapter, we present a generalized mean-field model as arguably the most simple dynamical model for frequency crosstalk between unforced and forced frequency components (Sec. 5.1). The control goal is to stabilize the unstable natural frequency. While the control based on linearized dynamics (Chapter 3) is shown to fail, MLC detects and exploits the frequency crosstalk mechanism in an unsupervised manner (Sec. 5.2). In Sec. 5.3, the derivation of the investigated model is sketched. This derivation contains the underlying approximations for the nonlinear control approaches, against which MLC is benchmarked in Sec. 5.4. The last two sections are analytical supplements for improved understanding of the model and the MLC control. These sections require background in methods of nonlinear oscillation [148] and nonlinear dynamics [125] and may be skipped during the first reading. Sec. 5.5 contains exercises for MLC control. A suggested reading (Sec. 5.6)

and an interview (Sec. 5.7) with Professor Mark Glauser, a pioneer in nonlinear modeling and feedback turbulence control, conclude this chapter.

5.1 Generalized mean-field system

In this section, we review a generalized mean-field model which explains how low- or high-frequency forcing stabilizes a self-amplified natural instability. The model has been used to explain the stabilizing effect of low-frequency forcing of a wake [209] and a resulting control design [6]. Similarly, the model has been applied to high-frequency forcing of a high-lift airfoil [176] and model-based control design [178]. Another application is an actuated swirling jet [201].

We refer to Sec. 5.3 for the derivation of the generalized mean-field model. The result is a four-dimensional model which describes the evolution of the mode amplitudes a_i , $i = 1, \dots, 4$ of a Galerkin expansion for the fluctuation. Here, a_1 , a_2 , is associated with the cosine and sine mode of natural vortex shedding and a_3 , a_4 describe analogous quantities for the periodically forced coherent structures. The system of ordinary differential equation reads

$$\frac{da_1}{dt} = \sigma_{\bullet} a_1 - \omega_{\bullet} a_2 \quad (5.1a)$$

$$\frac{da_2}{dt} = \sigma_{\bullet} a_2 + \omega_{\bullet} a_1 \quad (5.1b)$$

$$\frac{da_3}{dt} = \sigma_{\circ} a_3 - \omega_{\circ} a_4 \quad (5.1c)$$

$$\frac{da_4}{dt} = \sigma_{\circ} a_4 + \omega_{\circ} a_3 + g b \quad (5.1d)$$

$$\sigma_{\bullet} = \sigma_{\bullet\star} - \beta_{\bullet\bullet} r_{\bullet}^2 - \beta_{\bullet\circ} r_{\circ}^2 \quad (5.1e)$$

$$\omega_{\bullet} = \omega_{\bullet\star} + \gamma_{\bullet\bullet} r_{\bullet}^2 + \gamma_{\bullet\circ} r_{\circ}^2 \quad (5.1f)$$

$$\sigma_{\circ} = \sigma_{\circ\star} - \beta_{\circ\bullet} r_{\bullet}^2 - \beta_{\circ\circ} r_{\circ}^2 \quad (5.1g)$$

$$\omega_{\circ} = \omega_{\circ\star} + \gamma_{\circ\bullet} r_{\bullet}^2 + \gamma_{\circ\circ} r_{\circ}^2. \quad (5.1h)$$

The symbols are explained in Tab. 5.1.

The nonlinearity of Eq. (5.1) has two important effects. First, without forcing, $b \equiv 0$, the second oscillator vanishes, $a_3 = a_4 = 0$. Thus, equations (5.1a), (5.1b), (5.1e), and (5.1f) represent a Landau oscillator with linear oscillatory instability ($\sigma_{\bullet\star} > 0$) and a cubic damping ($\beta_{\bullet\bullet} > 0$). In other words, the first oscillator has a globally stable limit cycle as discussed in Sec. 4.4 for $b \equiv 0$. Second, with forcing at the eigenfrequency of the stable oscillator, i.e. $b = B \cos(\omega_{\circ\star} t)$, the amplitude of the second oscillator r_{\circ} grows in proportion to the forcing amplitude B , as the nonlinear terms of Eqs. (5.1c) and (5.1d) are assumed to vanish (see Tab. 5.1). The stabilizing effect of the second oscillator on the first one requires $\beta_{\bullet\circ} > 0$. Thus, fluctuation of the second oscillator reduces the growth rate of the first oscillator. The minimum

Table 5.1 Symbols of Sec. 5.1. The equations indicate the numerical values employed for the control problem.

Quantities related to the amplitude of the unstable oscillator (a_1, a_2)	
r_\bullet	: amplitude of the first oscillator
σ_\bullet	: growth rate
$\sigma_{\bullet\star} = 0.1$: initial growth rate near the fixed point $r_\bullet = 0$
$\beta_{\bullet\bullet} = 1$: parameter for growth-rate change of σ_\bullet due to r_\bullet
$\beta_{\bullet\circ} = 1$: parameter for growth-rate change of σ_\bullet due to r_\circ
Quantities related to the phase of the unstable oscillator (a_1, a_2)	
ϕ_\bullet	: phase of the first oscillator
ω_\bullet	: frequency (analog to r_\bullet for the amplitude)
$\omega_{\bullet\star} = 1$,	: initial frequency (analog to $\sigma_{\bullet\star}$ for the amplitude)
$\gamma_{\bullet\bullet} = 0$,	: parameter for frequency change due to r_\bullet (analog to $\beta_{\bullet\bullet}$)
$\gamma_{\bullet\circ} = 0$,	: parameter for frequency change due to r_\circ (analog to $\beta_{\bullet\circ}$)
Quantities related to the amplitude of the stable oscillator (a_3, a_4)	
r_\circ	: amplitude of the second oscillator
σ_\circ	: growth rate
$\sigma_{\circ\star} = -0.1$: initial growth rate near the fixed point $r_\circ = 0$
$\beta_{\circ\bullet} = 0$: parameter for growth-rate change of σ_\circ due to r_\bullet
$\beta_{\circ\circ} = 0$: parameter for growthrate change of σ_\circ due to r_\circ
$g = 1$: gain of control command
Quantities related to the phase of the stable oscillator (a_3, a_4)	
ϕ_\circ	: phase of the second oscillator
ω_\circ	: frequency (analog to r_\circ for the amplitude)
$\omega_{\circ\star} = 10$,	: initial frequency (analog to $\sigma_{\circ\star}$ for the amplitude)
$\gamma_{\circ\bullet} = 0$,	: parameter for frequency change due to r_\bullet (analog to $\beta_{\circ\bullet}$)
$\gamma_{\circ\circ} = 0$,	: parameter for frequency change due to r_\circ (analog to $\beta_{\circ\circ}$)

amplitude r_\circ for complete stabilization $r_\bullet = 0$ is $r_\circ = \sqrt{\sigma_{\bullet\star}/\beta_{\bullet\circ}}$, as can be derived from $\sigma_\bullet = 0$ in Eq. (5.1e). Physically, the forcing changes the base flow such that the production of the unstable coherent structures is reduced below the dissipative term.

In the following, Eq. (5.1) is simplified for the purpose of defining a control problem in which a high-frequency stable oscillator stabilizes a self-amplified amplitude-limited one. All coefficients which are not needed to illustrate the frequency crosstalk are set to zero, e.g. the Landau coefficients for the nonlinear terms of the second stable oscillator ($\beta_{\circ\circ} = \beta_{\circ\bullet} = \gamma_{\circ\circ} = \gamma_{\circ\bullet} = 0$) and for the frequency variation of the second oscillator ($\gamma_{\bullet\bullet} = \gamma_{\bullet\circ} = 0$). The small growth or decay rates of the oscillators are set to ± 0.1 , i.e. $\sigma_{\bullet\star} = 0.1$ and $\sigma_{\circ\star} = -0.1$. The large frequency of the second oscillator is set to $\omega_{\circ\star} = 10$. The remaining quantities, i.e. the frequency

and Landau coefficients of the first oscillator and the gain of the forcing term, are set to unity, $\omega_{\bullet\star} = \beta_{\bullet\bullet} = \beta_{\bullet\circ} = g = 1$. The parameter values are listed in Tab. 5.1

The resulting system reads:

$$\frac{da_1}{dt} = \sigma a_1 - a_2 \quad (5.2a)$$

$$\frac{da_2}{dt} = \sigma a_2 + a_1 \quad (5.2b)$$

$$\frac{da_3}{dt} = -0.1 a_3 - 10 a_4 \quad (5.2c)$$

$$\frac{da_4}{dt} = -0.1 a_4 + 10 a_3 + b \quad (5.2d)$$

$$\sigma = 0.1 - a_1^2 - a_2^2 - a_3^2 - a_4^2. \quad (5.2e)$$

For the initial condition at $t = 0$ we choose a point close to the unstable fixed point,

$$\mathbf{a}(0) = [a_1, a_2, a_3, a_4]^T(0) = [0.01, 0, 0, 0]^T. \quad (5.3)$$

The superscript ‘ T ’ denotes the transpose of the row vector.

The transient and actuated dynamics of Eq. (5.2) are illustrated in Fig. 5.1. The initial period shows an unforced transient towards the limit cycle. Then, actuation excites the stable oscillator which mitigates the first one via the growth rate.

The cost function to be minimized contains the average fluctuation level of the unstable oscillator

$$J_a = \overline{a_1^2 + a_2^2} \quad (5.4)$$

penalized by the actuation cost

$$J_b = \overline{b^2} \quad (5.5)$$

with penalization parameter γ ,

$$J := J_a + \gamma J_b = \overline{a_1^2 + a_2^2} + \gamma \overline{b^2} \stackrel{!}{=} \min. \quad (5.6)$$

The overbar denotes numerically an average over the time window $[20\pi, 220\pi]$, i.e. the average of a time-dependent function $f(t)$ reads

$$\overline{f(t)} := \frac{1}{200\pi} \int_{20\pi}^{220\pi} dt f(t).$$

The range of integration starts at $t_0 = 20\pi$, corresponding to 10 periods of the unstable oscillator, so that transients have time to die out. The upper integration bound is $t_1 = 220\pi$ to include 100 periods, which is sufficient for a statistical average. It should be noted that MLC requires only an approximately accurate ordering of the costs associated with the considered control laws. Hence, we refrain from using, say, 1000 periods to obtain slightly more accurate values.

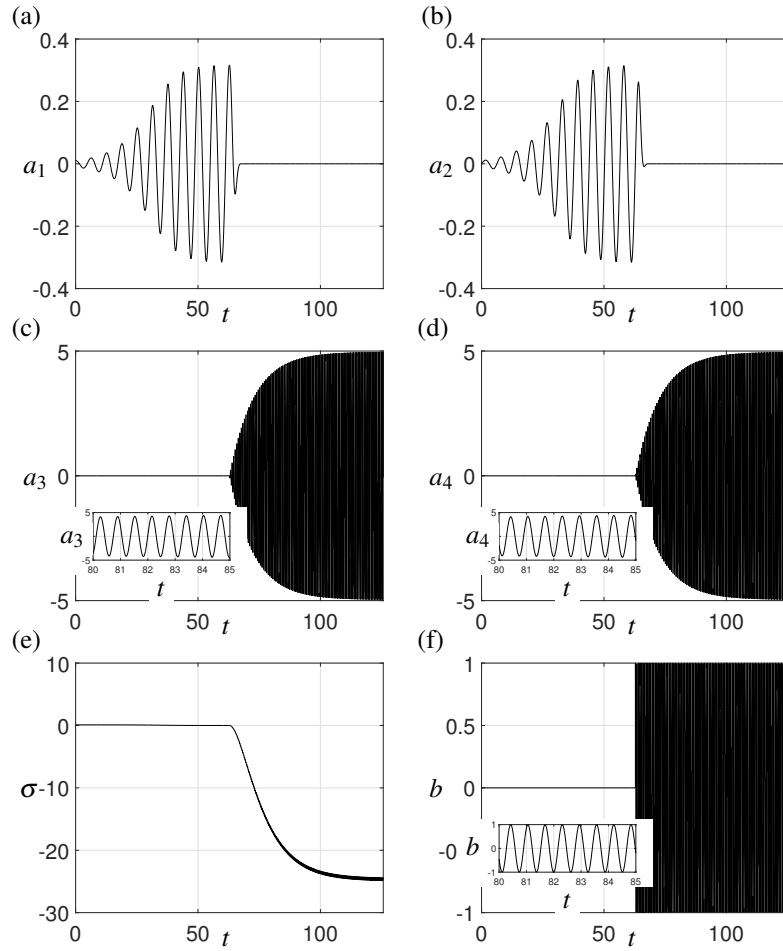


Fig. 5.1 Dynamics of the generalized mean-field model (5.2) with the initial condition (5.3). Periodic forcing $b = \cos(10t)$ is applied at $t \geq 20\pi$.

A canonical strategy for a stabilizing control employs a linearization of the evolution equation around the fixed point. The generalized mean-field model (5.2) has the fixed point $a_1 = a_2 = a_3 = a_4 = 0$. Linearizing around that point yields two uncoupled oscillators

$$\frac{da_1}{dt} = 0.1 a_1 - a_2 \quad (5.7a)$$

$$\frac{da_2}{dt} = 0.1 a_2 + a_1 \quad (5.7b)$$

$$\frac{da_3}{dt} = -0.1 a_3 - 10 a_4 \quad (5.7c)$$

$$\frac{da_4}{dt} = -0.1 a_4 + 10 a_3 + b. \quad (5.7d)$$

The amplitude of the first oscillator grows without bound while the second oscillator converges to its fixed point $a_3 = a_4 = 0$ without forcing. Evidently, the unstable oscillator cannot be stabilized by arbitrary actuation commands b , because the linearization has removed the pivotal nonlinear frequency crosstalk encoded in Eq. (5.1e). In terms of control theory from Chapter 3, the linearized system is not controllable.

5.2 Machine learning control

In this section, the control problem described in Sec. 5.1 is solved with MLC. Sec. 5.2.1 specifies the mathematical problem to be solved. In Sec. 5.2.2, the choice of parameters of MLC is outlined and motivated. The results are provided in Sec. 5.2.3.

5.2.1 Formulation of the control problem

The control problem for MLC consists of minimizing the cost function J (5.6) for the simplified generalized mean-field model (5.2) under initial condition (5.3). The penalization parameter is chosen to be $\gamma = 0.01$. The system is integrated numerically for a time range of $[20\pi, 220\pi]$, which allows for an unrecorded 10 period transient and evaluates 100 periods of the unstable oscillator deemed sufficient for representative statistics. At this point, we know that the linearized dynamics will not reveal the enabling frequency crosstalk mechanism and that an open-loop periodic forcing can completely stabilize the first oscillator. We search for an autonomous full-state feedback law minimizing the cost function,

$$b = K(\mathbf{a}) = K(a_1, a_2, a_3, a_4). \quad (5.8)$$

Thus, we explore all potential non-linear feedback mechanisms stabilizing the first oscillator. The optimization problem formally reads

$$K_{\text{opt}}(\mathbf{a}) = \underset{K(\mathbf{a})}{\operatorname{argmin}} J[K(\mathbf{a})] \Big|_{\substack{\text{subject to Eq. (5.2)} \\ \text{and initial condition (5.3)}}}, \quad (5.9)$$

where $K_{\text{opt}}(\mathbf{a})$ denotes the optimal control law which minimizes the cost. The dependency of the solution on the initial condition might be considered problematic and should normally be avoided. However, we recall that actuation will be evaluated after a long transient time. Secondly, the results have been found to hardly change after incorporating an ensemble of initial conditions in the regression problem (5.9).

5.2.2 MLC parameters

The function space of MLC is explored by using a set of elementary operations (+, −, ×, /) and transcendental (exp, sin, ln and tanh) functions. The functions are ‘protected’ to allow them to take arbitrary arguments in \mathbb{R} (e.g. a thresholding is achieved on denominators in divisions to avoid division by zero). Additionally, the actuation command is limited to the range $[-1, 1]$ to emulate an experimental amplitude-bounded actuator. Up to $N_g = 50$ generations comprising $N_i = 1000$ individuals are processed. The tournament size is $N_p = 7$, elitism is set to $n_e = 1$, the probabilities of replication, crossover and mutation are $P_r = 0.1$, $P_c = 0.6$ and $P_m = 0.3$ respectively (see Tab. 5.2).

Table 5.2 MLC parameters used for the control of the generalized mean-field model (5.2).

Parameter	N_i	P_r	P_m	P_c	N_p	N_e
Value	1000	0.1	0.3	0.6	7	1
Operations	+, −, ×, /, sin, exp, log, tanh					

5.2.3 MLC results

Figure 5.2 displays the MLC learning process associated with the optimization problem (5.9). The enforced ordering of the individuals with respect to their cost

$$J_1^j \leq J_2^j \leq \dots \leq J_{N_i}^j \quad j = 1, \dots, N_g$$

is evidenced in the j th column by increasing J -value with increasing i . The learning of increasingly better control laws with increasing generation number j can be seen from decreasing J values towards the right. In particular, elitism enforces that the cost of the best individual cannot increase,

$$J_1^1 \geq J_1^2 \geq \dots \geq J_1^{N_g}.$$

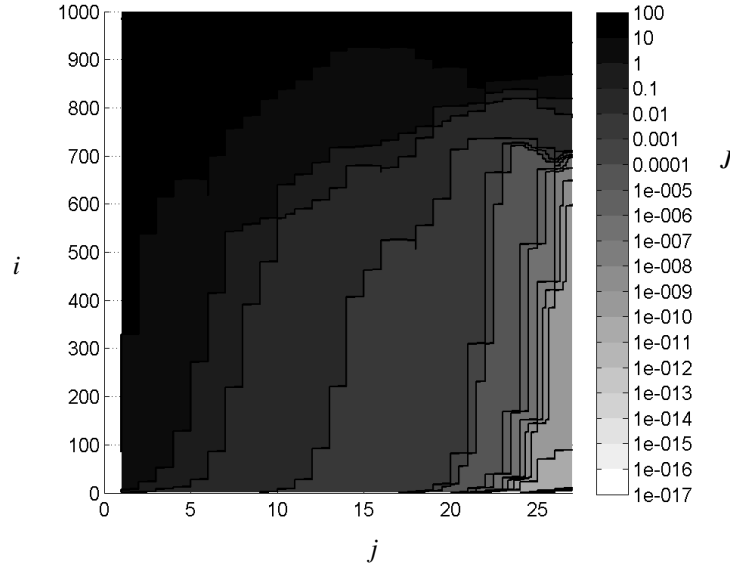


Fig. 5.2 MLC learning process for the control problem (5.9) with the generalized mean-field model. The abscissa displays the generation number j . The ordinate refers to the individual i . The background shows the value of the cost function J_i^j for each tested individual.

The ‘spectrogram’ of all computed J_i^j is visualized in Fig. 5.3. Each generation j is seen to consist of a large range of cost values.

The best individual $i = 1$ in the last generation $j = N_g$ defines solution of regression problem for the MLC feedback law (5.9). The corresponding actuated dynamics is depicted in Fig. 5.4. Intriguingly, MLC does not emulate periodic forcing with regular ‘soft’ excitation of the second oscillator. Instead, it chooses to stabilize the first oscillator by occasional hard ‘kicks’, i.e. by strongly exciting the second oscillator and decreasing the growth rate to low negative values.

The instance of these kicks is best appreciated in a logarithmic plot of the fluctuation levels of both oscillators (Fig. 5.5). The kicks occur at fluctuation levels of roughly 10^{-5} and last until this level has been decreased to around 10^{-40} or lower.

The MLC law solving the regression problem (5.9) is visualized in Fig. 5.6 as binary tree. The formula can be expressed as follows:

$$b = K_1(a_4) \times K_2(a_1, a_2, a_3, a_4) \quad (5.10)$$

with

$$K_1(a_4) = 5.475 \times a_4$$

and

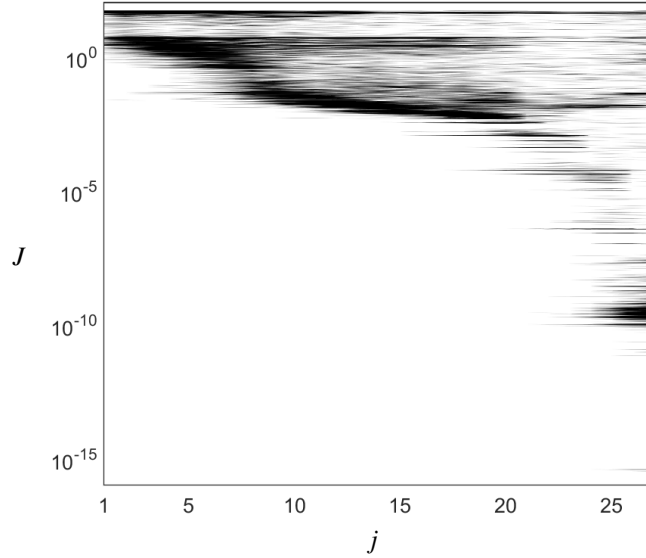


Fig. 5.3 Same MLC run as Fig. 5.2. Now, the J_i^j values, $i = 1, \dots, N_i$, for each generation j are indicated on a logarithmic ordinate scale.

$$\begin{aligned}
 K_2(a_1, a_2, a_3, a_4) = & \frac{\left(\frac{\left(\frac{a_4}{4.245} \right) \times \left(\sin\left(\tanh\left(\frac{-a_4}{-5.987} \right) \right) \right)}{\tanh(a_2)} + a_2 \right)}{\cos(3.053)} \\
 & \times \left(\frac{8.965}{\tanh(a_2)} + \frac{\frac{a_2}{\cos(3.053)}}{a_4 + \frac{\cos(-8.208)}{\log(a_3)}} \right) \\
 & \times \frac{\left(\frac{\left(\frac{a_1}{a_4} \right)}{\left(\frac{\left(\frac{\sin(a_4)}{-6.912 - (a_4)} \right) \times \left(\frac{\tanh((4.640) \times (a_2))}{(a_2) \times (a_4)} \right) \right)} \times \left(\frac{a_1}{(a_2) \times (a_4)} \right) \right)}{\frac{a_2}{a_1} + \tanh(a_2)} \times \left(\frac{a_1}{a_2} \right)}{-7.092}.
 \end{aligned}$$

The function $K_1(a_4)$ describes a phasor control that destabilizes the stable oscillator. The function $K_2(a_1, a_2, a_3, a_4)$ acts as a gain dominated by the energy of the unstable oscillator. This control law cannot be derived from a linearized model of the system. Moreover, (slightly) less energy is used as compared to the best periodic excitation.

A revealing illustration of the MLC control law in a four-dimensional space is a challenge. In the following, we propose a generic strategy. Let $p(\mathbf{a})$ be the probability density associated with the MLC-actuated dynamics (5.2). Thus, the expectation value of the actuation command $b = K(a_1, a_2, a_3, a_4)$ at given values a_1 and a_2 can be formally defined:

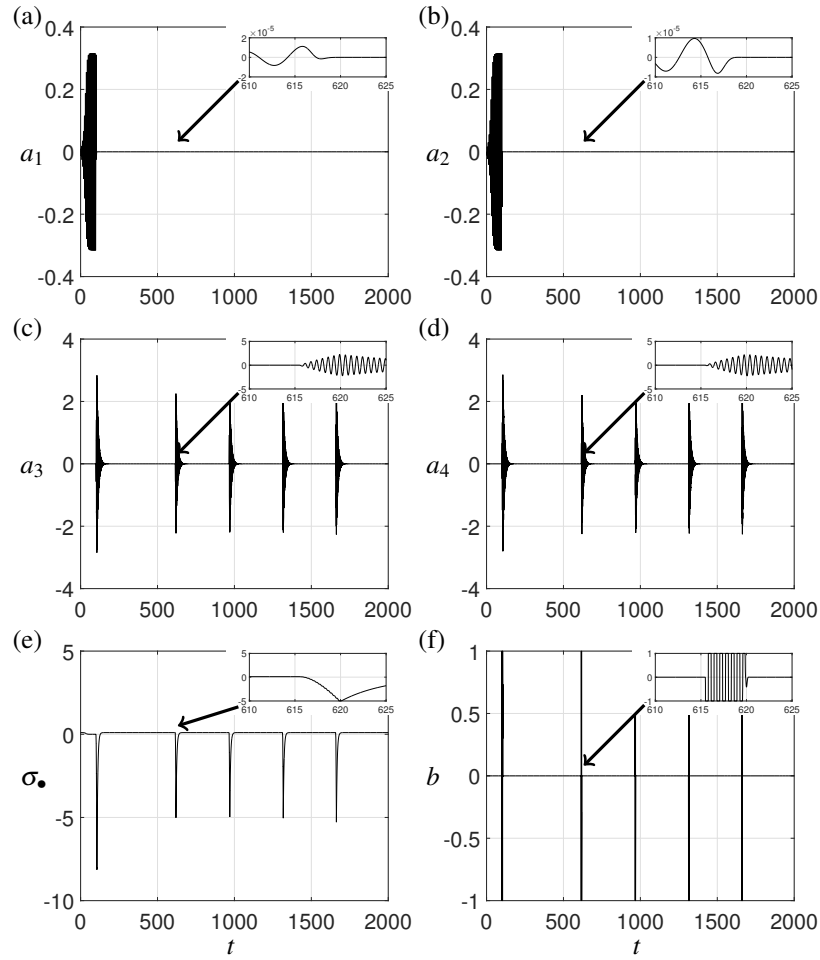


Fig. 5.4 Dynamics of the MLC-controlled generalized mean-field model (5.2).

$$\langle b \rangle_{\bullet} = \langle K \rangle_{\bullet} = \int \int p(a_1, a_2, a_3, a_4) K(a_1, a_2, a_3, a_4) da_3 da_4. \quad (5.11)$$

The analogous quantity for the second oscillator reads

$$\langle b \rangle_{\circ} = \langle K \rangle_{\circ} = \int \int p(a_1, a_2, a_3, a_4) K(a_1, a_2, a_3, a_4) da_1 da_2. \quad (5.12)$$

Figure 5.7 depicts this expectation value in the a_1 - a_2 plane. More precisely, we employ polar coordinates $a_1 = r_{\bullet} \cos \phi_{\bullet}$, $a_2 = r_{\bullet} \sin \phi_{\bullet}$, and plot the radius on a logarithmic scale. Thus, the phase associated with the expectation value of the control command b can be resolved even at small fluctuation values. Expectedly, no strong phase preference ϕ_{\bullet} for control action is apparent. Each period of the unstable os-

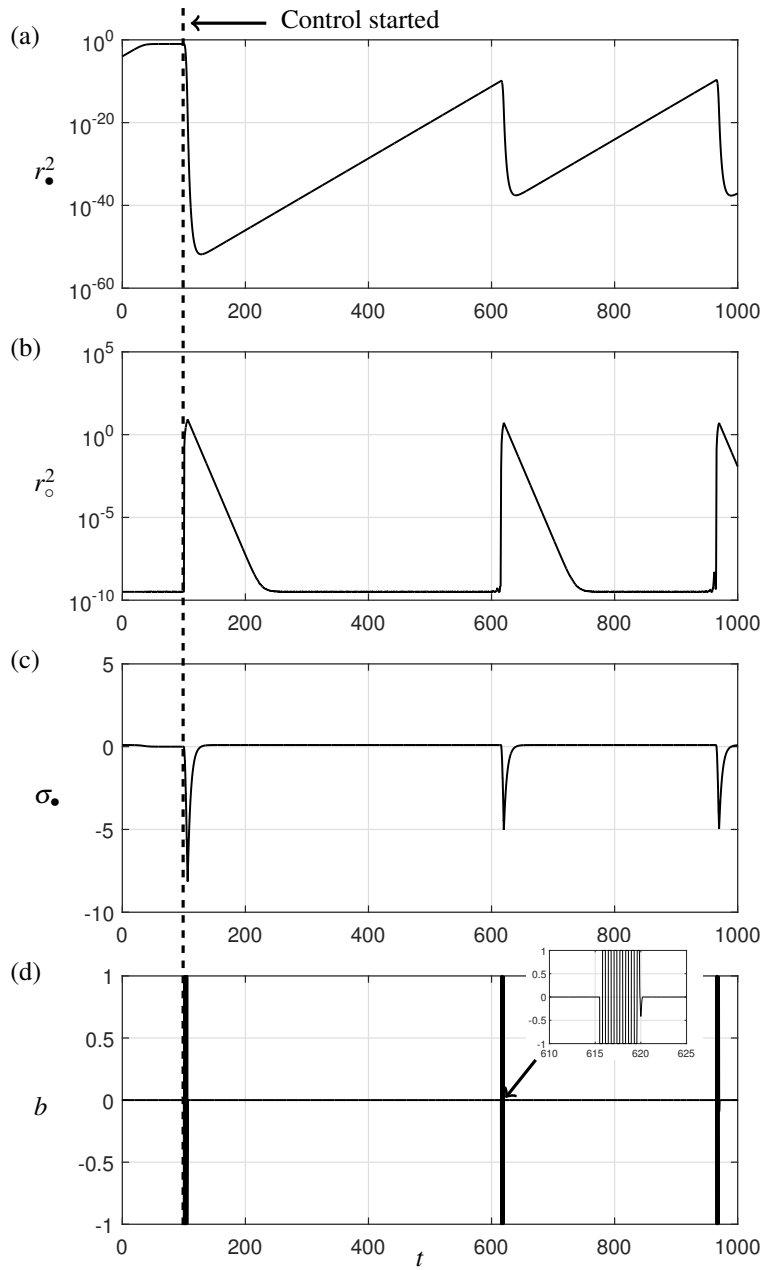


Fig. 5.5 Energy levels of the oscillators displayed in Fig. 5.4. When the energy contained in the first oscillator (top) is larger than 10^{-10} , the control (bottom) excites the second oscillator, and its energy grows to roughly 3 so that σ reaches approximately -6 ± 1 . This results in a fast decay of the energy in the first oscillator after which the control goes back to a “stand-by” mode.

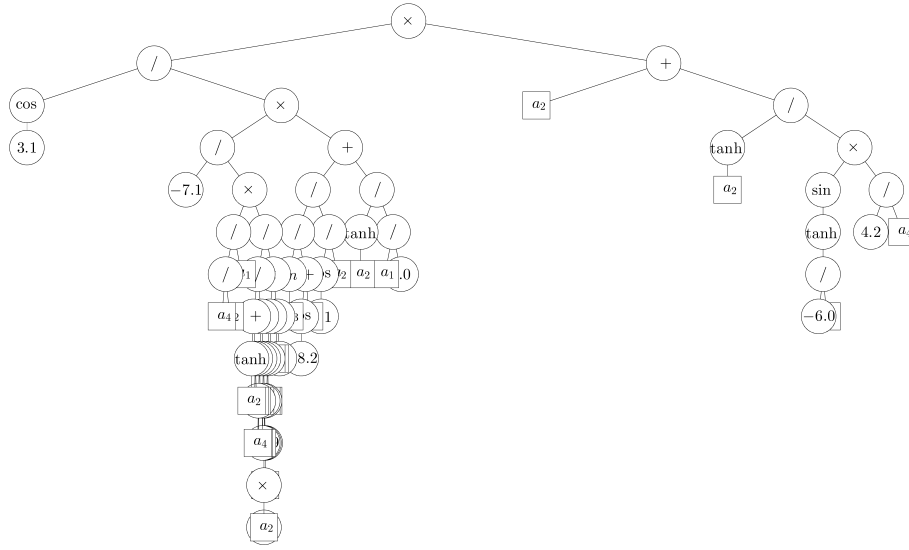


Fig. 5.6 Tree representation of the MLC law solving the regression problem (5.9) and used in Figs. 5.4 and 5.5.

cillator is associated with 20 sign changes of $\langle b \rangle$, because the actuation drives the stable high-frequency oscillator. The mostly white inner ring corresponds to regions without available data from the simulation. Figure 5.8 is an analogous visualization of the control law (5.12) for the a_3 - a_4 plane. This figure reveals the destabilizing factor $K_1(a_4)$ of the MLC control law (5.10).

5.3 Derivation outline for the generalized mean-field model

In this section, we outline the derivation of the generalized mean-field model of Sec. 5.1. The underlying approximations will be used in the alternative control design (Sec. 5.4). We consider an incompressible uniform flow around an obstacle in a steady domain Ω . The location is denoted by $\mathbf{x} = (x, y, z) \in \Omega$ and the time by t . Here, x, y, z are Cartesian coordinates. For a nominally two-dimensional shear flow, x points in the direction of the flow, y in the direction of the main gradient and z is the spanwise coordinate. The unit vectors in x, y and z directors are $\mathbf{e}_x, \mathbf{e}_y, \mathbf{e}_z$, respectively. Let $\mathbf{u} = (u, v, w)$ be the velocity and p be the pressure in this domain, respectively. Here, u, v, w are the Cartesian coordinates of the velocity. Let D and U represent the characteristic size and free-stream velocity, respectively. The incompressible Newtonian fluid is characterized by its density ρ and kinematic viscosity ν . The properties of the flow are determined by the Reynolds number $Re = UD/\nu$.

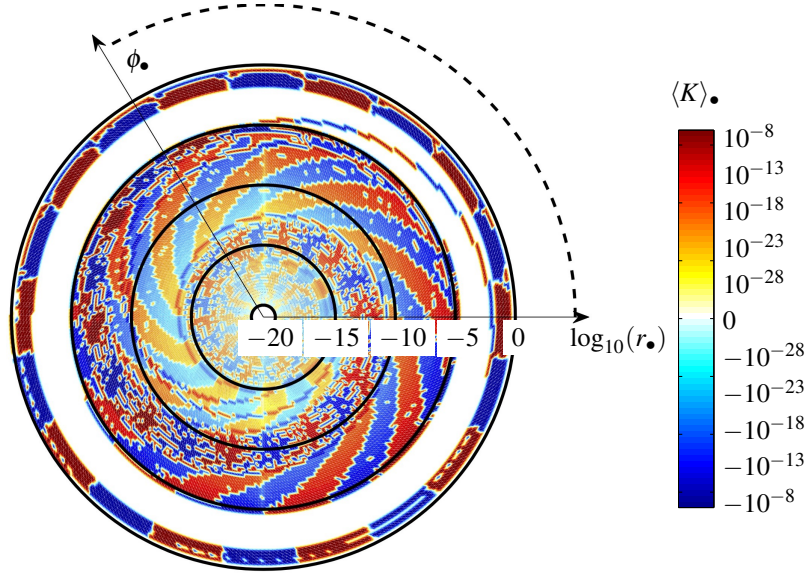


Fig. 5.7 Visualization of the MLC feedback law (5.9) in the a_1 - a_2 plane. The figure displays the expectation value (5.11).

In the following, all quantities are assumed to be non-dimensionalized with respect to the length scale D , the velocity scale U and density ρ .

The mass conservation or equation of continuity reads

$$\nabla \cdot \mathbf{u}(\mathbf{x}, t) = 0. \quad (5.13)$$

Here, ' ∇ ' represents the Nabla operator with respect to \mathbf{x} and ' \cdot ' an inner product. The momentum balance for an incompressible Newtonian fluid is given by the Navier-Stokes equations:

$$\partial_t \mathbf{u}(\mathbf{x}, t) + \mathbf{u}(\mathbf{x}, t) \cdot \nabla \mathbf{u}(\mathbf{x}, t) = -\nabla p(\mathbf{x}, t) + \frac{1}{Re} \Delta \mathbf{u}(\mathbf{x}, t). \quad (5.14)$$

The left-hand side corresponds to the acceleration of the fluid, the right-hand side contains the pressure and viscous forces. Here, $\nabla \mathbf{u}$ represents the velocity Jacobian, i.e. the outer product of ∇ with \mathbf{u} . Δ denotes the Laplace operator.

At the domain boundary $\partial\Omega$, the velocity satisfies Dirichlet conditions: it vanishes at the stationary body (no-slip condition) and assumes free-stream velocity at infinity,

$$\mathbf{u}(\mathbf{x}, t)|_{\partial\Omega} = \begin{cases} \mathbf{0} & \text{at the body;} \\ \mathbf{e}_x & \text{at infinity.} \end{cases} \quad (5.15)$$

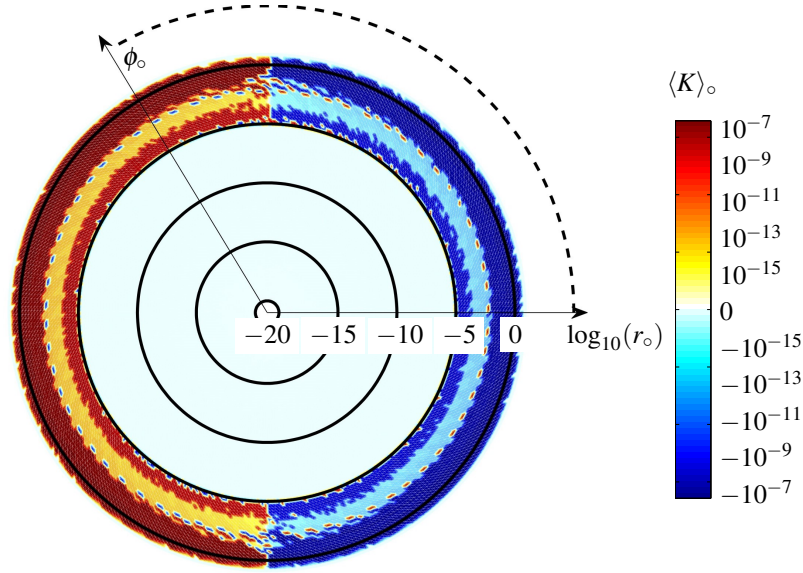


Fig. 5.8 Same as Fig. 5.7 but for (5.12) the a_3 - a_4 plane.

Let $\mathbf{v}(\mathbf{x})$ represent the initial condition at time $t = 0$,

$$\mathbf{u}(\mathbf{x}, 0) = \mathbf{v}(\mathbf{x}), \quad \forall \mathbf{x} \in \Omega. \quad (5.16)$$

Equations (5.13), (5.14), (5.15) and (5.16) define an initial boundary value problem which is assumed to have a unique solution under sufficiently smooth initial and boundary conditions. The uniqueness is mathematically proven for some two-dimensional flows [169] but is still an open problem for three-dimensional flows. It may be noted that examples of non-uniqueness are found for unsteady boundary conditions [224].

In the following, the derivation of a least-order model for flows dominated by two frequencies will be sketched. Details can be found in the original literature [176]. Generally, the Navier-Stokes equations are assumed to have one (and only one) steady solution $\mathbf{u}_s(\mathbf{x})$ with corresponding pressure field $p_s(\mathbf{x})$,

$$\mathbf{u}_s(\mathbf{x}) \cdot \nabla \mathbf{u}_s(\mathbf{x}) = -\nabla p_s(\mathbf{x}) + \frac{1}{Re} \Delta \mathbf{u}_s(\mathbf{x}). \quad (5.17)$$

There exist only few known exceptions of flows with no steady solution or multiple solutions which concern closed flows, like diffusor flow. Let $\mathbf{u}_\bullet(\mathbf{x}, t)$ denote the frequency contribution at angular frequency ω_\bullet of the unstable unforced flow. Similarly, let $\mathbf{u}_\circ(\mathbf{x}, t)$ represent the actuated contribution at angular frequency ω_\circ . The later component is assumed to vanish without forcing. ω_\bullet and ω_\circ are assumed

be incommensurable so that no lock-in occurs. Amplitudes and frequencies of both components may slowly vary with time. Correspondingly slow base flow changes due to the Reynolds stress are included in $\mathbf{u}_\Delta(\mathbf{x}, t)$. The resulting velocity decomposition reads

$$\mathbf{u}(\mathbf{x}, t) = \mathbf{u}_s(\mathbf{x}) + \mathbf{u}_\Delta(\mathbf{x}, t) + \mathbf{u}_\bullet(\mathbf{x}, t) + \mathbf{u}_\circ(\mathbf{x}, t). \quad (5.18)$$

In a simple, yet not unrealistic case, the unforced oscillation may be well approximated by a linear combination of two spatial modes $\mathbf{u}_1(\mathbf{x})$ and $\mathbf{u}_2(\mathbf{x})$ with time-dependent coefficients $a_1(t)$ and $a_2(t)$. These modes may be the first POD modes, the real and imaginary part of the dominant DMD mode [228, 237] or cosine and sine component of a Fourier mode at ω_\bullet . Similarly, the actuated oscillatory structures can be expected to be well resolved by a linear combination of two modes $\mathbf{u}_3(\mathbf{x})$ and $\mathbf{u}_4(\mathbf{x})$ with amplitudes $a_3(t)$ and $a_4(t)$. For simplicity, the modes are assumed to build an orthonormal basis without loss of generality, as they can easily be orthonormalized. Summarizing,

$$\mathbf{u}_\bullet(\mathbf{x}, t) = a_1(t) \mathbf{u}_1(\mathbf{x}) + a_2(t) \mathbf{u}_2(\mathbf{x}) \quad (5.19a)$$

$$\mathbf{u}_\circ(\mathbf{x}, t) = a_3(t) \mathbf{u}_3(\mathbf{x}) + a_4(t) \mathbf{u}_4(\mathbf{x}). \quad (5.19b)$$

Following Kryloff & Bogoliubov [167], the modal amplitudes a_i , $i = 1, \dots, 4$ are considered to be nearly pure harmonics, i.e.

$$a_1(t) = r_\bullet \cos \phi_\bullet \quad (5.20a)$$

$$a_2(t) = r_\bullet \sin \phi_\bullet \quad (5.20b)$$

$$a_3(t) = r_\circ \cos \phi_\circ \quad (5.20c)$$

$$a_4(t) = r_\circ \sin \phi_\circ \quad (5.20d)$$

$$\frac{d\phi_\bullet}{dt} = \omega_\bullet \quad (5.20e)$$

$$\frac{d\phi_\circ}{dt} = \omega_\circ, \quad (5.20f)$$

where the amplitudes r_\bullet and r_\circ and frequencies ω_\bullet and ω_\circ are slowly varying functions of time. It may be noted that (5.20) allows for arbitrary phase offsets. Thus, the Reynolds decomposition of the flow in Eq. (5.18) into a mean $\bar{\mathbf{u}}$ and a fluctuation \mathbf{u}' reads

$$\bar{\mathbf{u}}(\mathbf{x}, t) = \mathbf{u}_s(\mathbf{x}) + \mathbf{u}_\Delta(\mathbf{x}, t) \quad (5.21a)$$

$$\mathbf{u}'(\mathbf{x}, t) = \sum_{i=1}^4 a_i(t) \mathbf{u}_i(\mathbf{x}). \quad (5.21b)$$

The mean velocity is understood as an ensemble or short-term average to allow for slow unforced or actuated transients.

The base-flow deformation \mathbf{u}_Δ is inferred from the Reynolds equation, i.e. time-averaged Navier-Stokes equations (5.14). We substitute equation (5.21a) in (5.14) and subtract the steady Navier-Stokes equations (5.17). Averaging and neglecting

second-order terms in the base-flow deformation \mathbf{u}_Δ yields

$$\mathbf{u}_s \cdot \nabla \mathbf{u}_\Delta + \mathbf{u}_\Delta \cdot \nabla \mathbf{u}_s = -\nabla p + \frac{1}{Re} \Delta \mathbf{u}_\Delta - \nabla \cdot \overline{\mathbf{u}' \otimes \mathbf{u}'}. \quad (5.22)$$

In this equation, the spatio-temporal dependencies have been dropped for brevity. The right-most term is the Reynolds-stress force driving the base-flow deformation. The symbol ' \otimes ' emphasizes the outer product between the fluctuation vectors, leading to a matrix after the Nabla operator. Note that this system of partial differential equations is linear in \mathbf{u}_Δ and has a single forcing term. The pressure gradient can be considered as a projection on an incompressible velocity subspace, i.e. it neither interferes with the linearity in \mathbf{u}_Δ nor with the forcing term.

The Reynolds stress is given by

$$\overline{\mathbf{u}' \otimes \mathbf{u}'} = \frac{1}{2} r_\bullet^2 (\mathbf{u}_1 \otimes \mathbf{u}_1 + \mathbf{u}_2 \otimes \mathbf{u}_2) + \frac{1}{2} r_\circ^2 (\mathbf{u}_3 \otimes \mathbf{u}_3 + \mathbf{u}_4 \otimes \mathbf{u}_4) \quad (5.23)$$

exploiting (5.20). Evidently, the Reynolds-stress term has one contribution at the natural frequency ω_\bullet and another one at the actuated one ω_\circ . By the linear nature of (5.22), the base-flow deformation of both frequency components of the Reynolds stress are additive and can be associated with two shift-modes [196, 199]. Let $a_5 \mathbf{u}_5$ be the base-flow change corresponding to the natural frequency ω_\bullet and $a_6 \mathbf{u}_6$ the analog of the actuated frequency ω_\circ . From (5.22) and (5.23), we observe

$$a_5 = \alpha_\bullet r_\bullet^2 = \alpha_\bullet (a_1^2 + a_2^2) \quad (5.24a)$$

$$a_6 = \alpha_\circ r_\circ^2 = \alpha_\circ (a_3^2 + a_4^2). \quad (5.24b)$$

These equations define the mean-field manifolds hosting slow transients in the 6-dimensional state space $\mathbf{a} = [a_1, a_2, \dots, a_6]^T$.

The dynamic equations for a_i , $i = 1, 2, 3, 4$ can be obtained from the Navier-Stokes equations (5.14) exploiting the Kryloff-Bogoliubov approximation. Filtering (5.14) for ω_\bullet terms ignores all constant and quadratic terms since none of them can give rise to the frequency ω_\bullet . The projection onto \mathbf{u}_i for $i = 1, 2$ yields an oscillator which is base-flow dependent. A similar reasoning holds for the ω_\circ frequency. A volume force gives rise to an additive forcing term gb where b is the actuation command and g the gain. Without loss of generality, this forcing acts on the dynamic equation for a_4 , as the modes \mathbf{u}_i , $i = 3, 4$ can be rotated. Summarizing, we obtain (5.1).

5.4 Alternative control approaches

In the following, we will assess the efficiency of machine learning control and benchmark it against periodic forcing (Sec. 5.4.1), and against an energy-based closed-loop control design (Sec. 5.4.2). In Sec. 5.4.3, the efficiency of MLC on-off

control is assessed in an analytical framework. We rewrite the generalized mean-field model (5.2), giving all growth-rates symbols:

$$\frac{da_1}{dt} = \sigma_{\bullet} a_1 - a_2 \quad (5.25a)$$

$$\frac{da_2}{dt} = \sigma_{\bullet} a_2 + a_1 \quad (5.25b)$$

$$\frac{da_3}{dt} = \sigma_{\circ} a_3 - 10 a_4 \quad (5.25c)$$

$$\frac{da_4}{dt} = \sigma_{\circ} a_4 + 10 a_3 + b \quad (5.25d)$$

$$\sigma_{\bullet} = \sigma_{\star} - a_1^2 - a_2^2 - a_3^2 - a_4^2 \quad (5.25e)$$

$$\sigma_{\star} = 0.1 \quad (5.25f)$$

$$\sigma_{\circ} = -0.1. \quad (5.25g)$$

In the analytical computations, we will keep the growth-rate symbols of (5.25e), (5.25f) and (5.25g) to track the physical meaning of each formula.

5.4.1 Open-loop forcing

In this section, we minimize the cost functional (5.6) with (open-loop) periodic forcing. The stable oscillator is efficiently excited at its eigenfrequency

$$b = B \cos(10t). \quad (5.26)$$

The resulting fluctuation amplitude is proportional to the forcing amplitude, or, equivalently,

$$r_{\circ}^2 = \kappa B^2. \quad (5.27)$$

Here, κ is proportional to the reciprocal of the damping rate σ_{\circ} .

In the sequel, we apply the Kryloff-Bogoliubov approximation (5.20) for slowly varying amplitudes. Then, the first oscillator assumes a non-vanishing amplitude $r_{\bullet} > 0$ if and only if

$$\frac{dr_{\bullet}}{dt} = \sigma_{\bullet} r_{\bullet} = 0.$$

Equation (5.25e) implies the fluctuation level

$$J_a = r_{\bullet}^2 = \sigma_{\star} - r_{\circ}^2 = \sigma_{\star} - \kappa B^2. \quad (5.28)$$

The oscillation completely vanishes if $\sigma_{\bullet} \leq 0$ or, equivalently $B^2 \geq \sigma_{\star}/\kappa$. The associated actuation cost reads

$$J_b = \overline{b^2} = B^2/2. \quad (5.29)$$

Finally, the cost functional (5.6) reads

$$J = J_a + \gamma J_b = \sigma_* - \kappa B^2 + \frac{\gamma}{2} B^2 = \sigma_* + \left[\frac{\gamma}{2} - \kappa \right] B^2. \quad (5.30)$$

At vanishing actuation $B = 0$, we have the unactuated limit cycle and

$$J_\bullet = \sigma_*. \quad (5.31)$$

For later reference, we give this cost value the subscript ‘•’. Complete stabilization $r_\bullet = 0$ can be achieved with the minimum actuation level $B^2 = \sigma_*/\kappa$, corresponding to the cost

$$J_\circ = \frac{\gamma \sigma_*}{2 \kappa}. \quad (5.32)$$

For later reference, this cost value has the subscript ‘o’. Intermediate actuation amplitudes $0 < B^2 < \sigma_*/\kappa$ yield intermediate costs. The trade-off between achieved stabilization and actuation cost is easily appreciated in the Pareto diagram in Fig. 5.9.

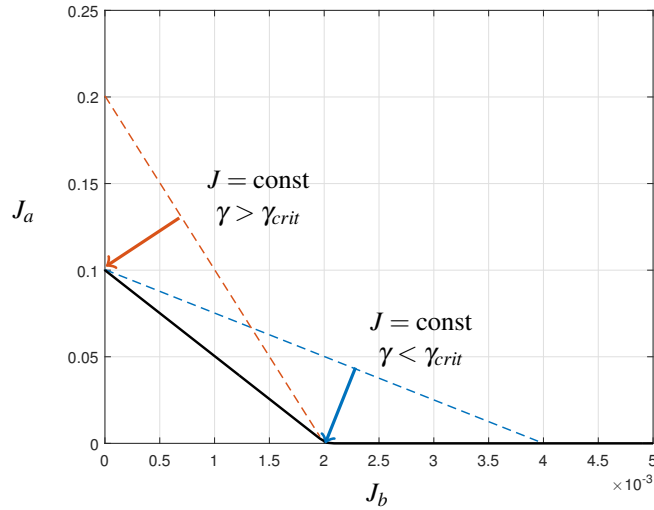


Fig. 5.9 Pareto diagram for the stabilization of the generalized mean-field model (5.2). The black line denotes equilibrium points for open-loop forcing from the unforced limit cycle ($B = 0$) to complete stabilization $r_\bullet = 0$ according to Eq. (5.30). For more details see text.

Intriguingly, the solution of the optimization problem depends discontinuously on γ . If $\gamma < \gamma_{\text{crit}} := 2 \kappa$, $J_\circ < J_\bullet$ and minimization of the cost functional leads to complete stabilization of the unstable oscillator. If $\gamma > \gamma_{\text{crit}}$, minimization leads to the unactuated limit cycle with vanishing forcing. If $\gamma = \gamma_{\text{crit}}$, any forcing $0 \leq B^2 \leq \sigma_*/\kappa$ leads to the same J and the minimization problem has no unique solution. The γ

chosen in Sec. 5.2.1 was subcritical. Hence, MLC has targeted complete stabilization.

The periodic forcing constitutes a benchmark against which closed-loop control can be measured. Periodic forcing is easily realizable in any system and any experiment. The optimal forcing parameters can be determined, e.g. by gradient search or extremum/slope seeking. The corresponding Pareto diagram illustrates which level of stabilization can be achieved at which actuation cost. In principle, the best closed-loop control may be inside or outside the triangle $J_a + J_b \leq J_\bullet$. There is no a priori guarantee that closing the loop will beat periodic forcing. We shall explore this aspect in later sections.

We shall not pause to inquire if Eq. (5.26) defines the best open-loop actuation command $b = K(t)$ with respect to the cost-functional.

5.4.2 Closed-loop forcing

In this section, we design a closed-loop forcing (5.8) which stabilizes the first oscillator. As seen in Sec. 5.1, linear control theory is not applicable. Instead, we employ an energy-based control design under the Kryloff-Bogoliubov approximation (5.20).

The starting point is the fluctuation level

$$J_a = \overline{r_\bullet^2} = r_\bullet^2 = a_1^2 + a_2^2.$$

We assume an average over an infinite time window, i.e. we neglect transient behavior. Thus, the averaging sign over r_\bullet^2 is redundant under the Kryloff-Bogoliubov approximation.

Differentiating with respect to time and employing the evolution equations (5.25a), (5.25b) and dividing by 2 yields

$$r_\bullet \frac{r_\bullet}{dt} = a_1 \frac{a_1}{dt} + a_2 \frac{a_2}{dt} = \sigma_\bullet r_\bullet^2.$$

Stabilization of the first oscillator implies $r_\bullet = 0$ by definition and $\sigma_\bullet < 0$ for stability under noise. From Eq. (5.25e), this requires an excitation of the second oscillator to the level $r_\circ^2 \geq \sigma_\bullet$. It should be noted that the Kryloff-Bogoliubov assumption implies slowly varying amplitudes and accounting for time-averaging effects is not necessary. Hence, stabilization of the first oscillator implies a destabilizing control for the second one. We proceed as with the first oscillator, and differentiate

$$r_\circ^2 = a_3^2 + a_4^2$$

with respect to time, employ Eqs. (5.25c), (5.25d), and divide by 2 to obtain

$$r_\circ \frac{r_\circ}{dt} = a_3 \frac{a_3}{dt} + a_4 \frac{a_4}{dt} = \sigma_\circ r_\circ^2 + a_4 b. \quad (5.33)$$

For limit-cycle behavior, the average energy $\overline{a_4 b}$ needs to overcome the dissipation $\sigma_o r_o^2$.

$$0 = \sigma_o r_o^2 + \overline{a_4 b}. \quad (5.34)$$

We see that b contributes to the fluctuation energy only if it has the same sign as a_4 . This is satisfied by the linear feedback ansatz

$$b = K a_4, \quad (5.35)$$

with $K > 0$. The sinusoidal behavior (5.20d) allows one to estimate the actuation power with $\overline{a_4 b} = K \overline{a_4^2} = K r_o^2 / 2$. Thus, the steady-state gain can be derived from Eq. (5.34) to be $K = -2\sigma_o$, leading to

$$b = -2\sigma_o a_4. \quad (5.36)$$

This control law implies a vanishing growth rate, or $r_o = \text{const}$, where the constant is determined by the initial conditions. In other words, Eq. (5.36) does not drive the actuated dynamics towards specific limit-cycle radii.

In contrast, the nonlinear gain

$$b = K a_4, \quad \text{where} \quad K = -2\sigma_o + \sigma_* - r_o^2 \quad (5.37)$$

ensures that the minimal fluctuation level $r_o^2 = \sigma_*$ is stabilized. Substituting Eq. (5.37) in Eq. (5.33) and averaging over one period yields the following amplitude equation for the actuated dynamics:

$$\frac{dr_o}{dt} = \frac{1}{2} r_o (\sigma_* - r_o^2).$$

A fluctuation level that is too small (large) is compensated for by a larger (smaller) gain K as compared to the equilibrium value $-2\sigma_o$.

The above nonlinear feedback law (5.37) stabilizes the desired fluctuation level of the second oscillator but does not compensate for any error of the dynamics. The alternative law

$$b = K a_4 \quad \text{where} \quad K = -2\sigma_o + 10 r_o^2 \quad (5.38)$$

increases the gain sharply if the first oscillator is not stabilized.

In summary, the discussed nonlinear feedback laws lead to the optimal periodic forcing of Sec. 5.4.1 with the same cost functional. There is no steady-state performance benefit from using the discussed closed-loop control. This equivalence is not overly surprising as the very Kryloff-Bogoliubov assumption implies nearly periodic behavior of both oscillators. Yet, feedback can buy an improved stabilization in case of model uncertainty, e.g. accounting for unknown errors of the growth rates. Accounting for model errors is one of the very purposes of feedback.

5.4.3 Short-term forcing

In this section, we analytically assess the benefits from strong short-term periodic forcing (5.26) to reduce r_\bullet from $r_{\max} \ll \sqrt{\sigma_\star}$ to r_{\min} . This forcing is an idealization of the MLC law in Sec. 5.2. Here, r_{\max} is at least 4 orders of magnitude below its unforced limit-cycle value.

Let $\sigma_a < 0$ be the commanded decay rate during periodic forcing. According to Eq. (5.25e),

$$\sigma_a = \sigma_\star - r_\bullet^2 - r_\circ^2 \approx 0.1 - r_\bullet^2.$$

In this approximation, we ignore $r_\bullet^2 \leq r_{\max}^2 \ll \sigma_\star$ by the smallness assumption of r_{\max} . In addition, we neglect transient effects, as the second oscillator is forced over many cycles. Then, we can use the quasi-equilibrium assumption of Sec. 5.4.1 and arrive at

$$\sigma_a = \sigma_\star - \kappa B^2. \quad (5.39)$$

By similar reasoning, the unactuated growth rate reads

$$\sigma_u = \sigma_\star, \quad (5.40)$$

since r_\circ vanishes without actuation and r_\bullet is assumed to be negligible as compared to $\sqrt{\sigma_\star}$. Summarizing,

$$\frac{dr_\bullet}{dt} = \sigma_\bullet r_\bullet \quad \text{where} \quad \sigma_\bullet = \begin{cases} \sigma_a & \text{during actuation} \\ \sigma_\star & \text{otherwise} \end{cases}. \quad (5.41)$$

The time interval τ_a for the actuation is given by

$$-\sigma_a \tau_a = \ln \left[\frac{r_{\max}}{r_{\min}} \right]. \quad (5.42)$$

Similarly, the time for the unforced period τ_u reads

$$\sigma_\star \tau_u = \ln \left[\frac{r_{\max}}{r_{\min}} \right]. \quad (5.43)$$

The period for one on-off cycle is the sum:

$$\tau = \tau_a + \tau_u = \left[-\frac{1}{\sigma_a} + \frac{1}{\sigma_\star} \right] \ln \left[\frac{r_{\max}}{r_{\min}} \right]. \quad (5.44)$$

The ratio of the actuation time with respect to this period is

$$\frac{\tau_a}{\tau} = \frac{\frac{-1}{\sigma_a}}{\left[\frac{1}{\sigma_\star} - \frac{1}{\sigma_a} \right]} = \frac{1}{\left[1 - \frac{\sigma_a}{\sigma_\star} \right]} = \frac{1}{\left[1 - \frac{\sigma_\star - \kappa B^2}{\sigma_\star} \right]} = \frac{\sigma_\star}{\kappa B^2}. \quad (5.45)$$

The stronger the actuation, the smaller the relative actuation time. Note that the ratio does not depend on the limits imposed on r_\bullet .

Following earlier reasoning, the stabilization can be considered complete, since $J_a = r_\bullet^2 \ll J_\bullet$. The only contribution to the cost functional comes from the actuation. The average actuation level is the product between the relative actuation time τ_a/τ and the maximum actuation level $B^2/2$:

$$J = \overline{\gamma b^2} = \gamma \frac{\tau_o}{\tau} \frac{B^2}{2} = \gamma \frac{\sigma_\star}{\kappa B^2} \frac{B^2}{2} = \gamma \frac{\sigma_\star}{2\kappa} = J_\bullet. \quad (5.46)$$

Intriguingly, the cost of on-off actuation is identical to the best periodic forcing J_\bullet of Eq. (5.32). Numerically the MLC control law is found to be slightly better due to a finite-window effect. The difference decreases with increasing integration time. MLC exploits even this finite-window effect for closed-loop control design.

The decision to turn actuation on or off in the framework of full-state feedback (5.8) is far from obvious. One ‘relay switch’ using the Heaviside function H reads

$$\chi = H(r_\bullet - r_{\max}) - H(r_{\min} - r_\bullet) + H(-\sigma_\star + r_o^2).$$

If $r_\bullet > r_{\max}$, $\chi > 0$ and actuation is turned on. If $r_\bullet < r_{\min}$, $\chi \leq 0$ and actuation is turned off. At intermediate values $r_{\min} < r_\bullet < r_{\max}$, χ is kept on if actuation has a damping effect (actuated transient) and χ is kept off if the second oscillator is not excited enough. MLC has constructed such a switch for an incremental finite-window performance benefit. This is an impressive performance of an automated control design.

5.5 Exercises

Exercise 5–1: Consider the following three coupled oscillators

$$\frac{da_1}{dt} = \sigma_1 a_1 - a_2 \quad (5.47a)$$

$$\frac{da_2}{dt} = \sigma_1 a_2 + a_1 \quad (5.47b)$$

$$\frac{da_3}{dt} = \sigma_2 a_3 - \pi a_4 \quad (5.47c)$$

$$\frac{da_4}{dt} = \sigma_2 a_4 + \pi a_3 + b \quad (5.47d)$$

$$\frac{da_5}{dt} = \sigma_3 a_5 - \pi^2 a_6 \quad (5.47e)$$

$$\frac{da_6}{dt} = \sigma_3 a_6 + \pi^2 a_5 + b \quad (5.47f)$$

$$\sigma_1 = -r_1^2 + r_2^2 - r_3^2 \quad (5.47g)$$

$$\sigma_2 = 0.1 - r_2^2 \quad (5.47h)$$

$$\sigma_3 = -0.1, \quad (5.47i)$$

where $r_1^2 := a_1^2 + a_2^2$, $r_2^2 := a_3^2 + a_4^2$, and $r_3^2 := a_5^2 + a_6^2$. Explore the unforced behavior ($b \equiv 0$) by numerical simulations. Explain the coupling between the oscillators in words. Derive an analytical solution of the unforced system (5.47).

Exercise 5–2: Stabilize the first oscillator of Eq. (5.47) with a full-state feedback law $b = b(\mathbf{a})$ by minimizing

$$J = \overline{r_1^2} + \overline{b^2}. \quad (5.48)$$

Linearize (5.47) and design a corresponding LQR controller (see Chapter 4). Explain the results.

Exercise 5–3: Stabilize the first oscillator of (5.47) with a full-state nonlinear feedback law $b = b(\mathbf{a})$ by minimizing J of Eq. (5.48). Use the Kryloff-Bogoliubov approximation of Sec. 5.4. Explain the results.

Exercise 5–4: Find the best periodic actuation

$$b = B \cos(\omega t). \quad (5.49)$$

- Set $B = 1$ and perform a frequency scan of ω , which effects all oscillator amplitudes r_1, r_2, r_3 . Can you explain the extrema of the amplitudes?
- Determine analytically the best control law with smallest J of Eq. (5.48), i.e. determine the best B and Ω . Justify physically why these parameters are optimal (no proof needed). Is this open-loop control better or worse than the closed-loop of the previous exercise? Why?

Exercise 5–5: Apply MLC with the same parameters as in Sec. 5.2. Take

$$\mathbf{a}(0) = [0.1, 0, 0.1, 0, 0.1, 0]^T$$

as initial condition, integrate 20 periods of the first oscillator ($t \in [0, 20\pi]$) and evaluate the cost functional in the next 100 periods ($t \in [20\pi, 220\pi]$). Bound the actuation by the interval $[-1, 1]$. Can you explain the control law and solution? How does it compare with the closed-loop and open-loop solution of Exercises 3 and 4?

5.6 Suggested reading

Texts

- (1) **Turbulence, Coherent Structures, Dynamical Systems and Symmetry**, by P. Holmes, J. L. Lumley, G. Berkooz and C. W. Rowley, 2012 [138].
The book represents a classic of POD Galerkin models of turbulent flows from the pioneers of the field.
- (2) **Nonlinear Ordinary Differential Equations**, by D. W. Jordan and P. Smith, 1988 [148].
This textbook provides an easily comprehensible and thorough introduction into nonlinear dynamics and the Kryloff-Bogoliubov approximation used in this chapter.

Seminal papers

- (1) **Rods and plates: series occurring in various questions regarding the elastic equilibrium of rods and plates (translated)**, by B. G. Galerkin 1915 [109].
This seminal paper proposed an elegant method for deriving ordinary differential equations (ODE) from partial differential equations (PDE) using modal expansions. This Galerkin method has become a very foundation for over 100 years of research in computational methods for PDEs and in reduced-order modeling.
- (2) **Nonlinear stability theory**, by J. T. Stuart, 1971 [256].
This review article summarizes the development of mean-field models which were pioneered by the author and which are the foundation of this chapter. J. T. Stuart was the first to derive a low-order Galerkin model explaining the coupling between fluctuation and base flow.

5.7 Interview with Professor Mark N. Glauser

Mark Glauser is Professor of Mechanical and Aerospace Engineering and Associate Dean for Research and Doctoral Programs at the College of Engineering and Computer Science of Syracuse University, NY, USA. He is also Professor of Physics at the College of Arts and Sciences of the same university.

As Associate Dean for Research and Doctoral Programs within the College of Engineering and Computer Science, Prof. Glauser is responsible for overseeing current research activities and coordinating the development of the college's future research portfolio. In his own research portfolio, Prof. Glauser, along with his co-workers, post-docs, graduate and undergraduate students, conducts major experimental, computational and theoretical efforts to apply low-dimensional models to turbulent and transitional flows for understanding and control. Flows studied range from high speed aerospace type applications to those around thermal breathing manikins within the micro-environment. Recent work involves developing closed-loop flow control methods based on the use of Proper Orthogonal Decomposition (POD) and Stochastic Measurement (SM) for various turbulent flows including that over a NACA 4412 airfoil, high speed (high subsonic and supersonic) turbulent jets for noise reduction/enhanced mixing, 3D separated flow control over turrets for improving aero-optics and for improving efficiency and reducing unsteady loading on large wind turbines. Prof. Glauser has or is currently serving as: a member of the US Army Science Board where he just finished co-chairing a 2014-15 study on The Future of Army Aviation; as a member of the NASA Langley Fundamental Aerodynamics Peer Review Panel (2014, 2009); Associate Editor, AIAA Journal (2007-2016); Program Manager for the Turbulence and Internal Flows Program at the US Air Force Office of Scientific Research (AFOSR) from 1996-1999; meeting Chair for the 56th APS Annual Meeting of the Division of Fluid Dynamics, November 2003; Technical Chair for the AIAA Summer Fluid Dynamics Meeting, June 2006; an ABET evaluator for Aerospace Engineering programs since 2004; and an ABET EAC member (2013-2015). Prof. Glauser has obtained more than 12 Million dollars in research funding as PI or Co-PI from AFOSR, NSF, NASA, EPA, DoE, Dantec, GE, United Technologies, Spectral Energies, Clear Science Corporation and others. Prof. Glauser has published more than 110 peer-reviewed publications and conference proceedings and has presented more than 100 invited presentations and keynote talks worldwide. Over the past 25+ years he has mentored several postdocs and more than 30 Ph.D. and MS students. Prof. Glauser is a Fellow of the American Institute of Aeronautics and Astronautics, the American Society of Mechanical Engineers, the American Physical Society, and the Institute of Physics (UK). In 1995, he was a



Fulbright Scholar in Poitiers, France. Prof. Glauser received his BS (1982) and his Ph.D. (1987) from the Department of Mechanical and Aerospace Engineering of the University at Buffalo SUNY, NY, USA.

Authors: Dear Mark, you have been one of few pioneers in reduced-order modeling of turbulence, particularly for application-related experiments. What did you learn about flow control? Where do you still see rewarding research opportunities for young talented researchers?

Prof. Glauser: Beginning with the ActiveWing dynamic separation flow work (joint with Lumley, Leibovich and Berkooz, see Taylor and Glauser 2004 [260]) in the mid 1990s to the NACA 4412 closed-loop separation control work (see Pinier et al. 2007 [214]), to the aero-optics related turret separation control work (Wallace et al 2012 [273] and [264]) and to our more recent high speed jet control work [175, 26], I have learned that this is a hard problem and that the most progress is made when there is strong interaction between controls and fluids experts with a nice mix of experimentalists, theorists and computationalists from both fields.

It is my view that there are many rich and interesting closed loop flow control problems in the Energy and Aerospace sector and beyond. Reducing unsteady loading on wind turbines with large wind farms for example is an important potential application for closed loop flow control. With the world-wide explosion of Unmanned Ariel Systems this would seem to be an especially important area due to the need for advanced intelligent platforms that can operate safely in complex and uncertain environments (gusts and other extreme weather events, degraded visual environments and etc.)

Authors: You have also pioneered closed-loop turbulence control in real-world experiments. You have decided to perform a model-free control and did not use your reduced-order models for control design. Why?

Prof. Glauser: This has not been entirely the case. The closed-loop flow control work on turrets for Aero-optics applications incorporated models (joint work with Hal Carlson, see for example Wallace et al. 2012 [273]) and conceptually the early ActiveWing work with Lumley and Leibovich had modeling at its core. Frankly, it is just not always possible to have a full team to handle the challenges associated with bringing in the models due to funding constraints. In addition, the complex experiments we run in our lab are very challenging and it is generally not feasible to have a Ph.D. student do both the modeling and experiments and have them graduate in a reasonable time frame. With the Aero-optics work where modeling was incorporated we were fortunate enough to have a strong team across the board. In addition, the experiments we have been doing in jets are very high Reynolds number and hence the flows themselves are very high dimensional so model development is more difficult than for the lower dimensional separation flow control problems we have performed. The bottom line, the flows examined and availability (or lack of) of a complete team have played the key

roles in the level of modeling that we have been able to successfully incorporate.

Authors: Yet, the literature contains myriad of studies on model-based flow stabilization in numerical simulations. What is the difference between experimental and numerical control?

Prof. Glauser: This is partially answered in my response to the question above. Typically many of the numerical simulation-based flow control studies have been at lower Reynolds number with relatively simple boundary conditions. Thankfully the simulation tools are improving and we are starting to reach more realistic Re numbers with LES. The experimental tools are improving as well, including powerful Time Resolved PIV tools. The best approach, if possible is to work the problem from both sides, using the high spatial resolution of simulations to provide key guidance to experiments. This can include, for example, simulation-guided placement of sensors and actuators along with key time and spatial scales at which to drive the flow to achieve the desired control objectives. Simulation derived low-dimensional models, even if somewhat limited, can be used, at least as a starting point, or perhaps fused with experimentally derived models, to provide the model-based control.

Authors: Where do you see the range of applicability of model-based control which has motivated this chapter?

Prof. Glauser: In principle, model-based control can and should, if possible, be used across the range of applications experienced in the energy and aerospace sector and beyond.

Authors: You have been enthusiastically supporting computer science methods for years. Can you give us an idea about evolving machine learning applications in turbulence control in the coming decade?

Prof. Glauser: It is my view that machine learning methods must be brought to bear on the difficult nonlinear stochastic problem we are trying to control if we are going to make real progress. However, I view machine learning as a complement to our Navier-Stokes based tools and not an either-or scenario. All of it should be thought of and used as "information" to help solve the nonlinear control problems we are faced with.

Authors: Which fluid dynamics expertise is not likely to be replaced by machine learning in the coming decade?

Prof. Glauser: We will continue to need theorists, experimentalists and computationalists, all who, however, in my view, will need to have a working knowledge of the latest math and computer science tools for both understanding and controlling high dimensional non-linear time dependent stochastic systems such as turbulence.

Authors: We look forward to your next breakthroughs in experimental turbulence control and thank you for this interview!